Pergamon *Ocean Engng*. Vol. 24, No. 2, pp. 95-110, 1997

S0029-8081(96)00008-8

WAVE INDUCED MOTION OF FLIP

Jerome A. Smith * and Karl F. Rieder

Scripps Institution of Oceanography, University of California at San Diego, La Jolla, CA 92093-0213 U.S.A.

(Received ; accepted in final form)

Abstract—The value of data gathered from R/P FLIP is enhanced if the motion of FLIP is described. At surface wave frequencies, FLIP's motion can be estimated from measurements of apparent acceleration and heading. This minimal set of measurements is often available in past data sets (e.g., from the Surface Wave Process Program, or SWAPP). In addition, the accelerometer data is often of superior quality, with less noise and greater dynamic range than other available data. The challenge is to partition the motion between true horizontal acceleration and tilt. For this, a quasi-linear dynamic model of FLIP's response to forcing by surface waves is developed, including added mass and drag terms. The model is refined on the basis of comparisons with more extensive motion data, gathered over a variety of wind and wave conditions: estimates of FLIP's tilt from measurements of the earth's magnetic flux vector, combined with gyro-compass heading, and horizontal velocity at 35 m estimated from surface-scanning Doppler sonars. The overall agreement between model estimates derived from accelerometer data and the others is good.

1. INTRODUCTION

The research platform *FLIP* (Floating Instrument Platform) is a 108 m long vessel, which 'flips' to a vertical orientation on station. When vertical, it provides a stable platform from which to make oceanographic measurements (Figure 1). For example, as part of the Surface Wave Process Program (SWAPP), *FLIP* was moored at 35°N, 127°W, roughly 500 km off the coast of California, from February 24,1990 through March 18, 1990. The objective of this program was to measure surface waves and wave-related flows in the mixed layer, and to relate these to forcing by buoyancy fluxes and wind stress (Weller et al., 1991).

Although *FLIP*'s motion is generally small (e.g., a few degrees of tilt), knowledge of this motion could help in several ways. During SWAPP, for example, specialized Doppler sonars were deployed to measure the surface water velocity along several lines radiating from *FLIP*. These permit estimation of both directional surface wave spectra and lower frequency motions at the surface (Smith, 1992; Smith and Bullard, 1995). The directional surface wave estimates could be improved if *FLIP*'s response to the waves could be incorporated. *FLIP*'s motion also affects wind measurements made with sonic anemometers and surface elevation measurements made with resistance wires. The wind measurements are used to calculate the wind stress, or momentum flux from the atmosphere to the ocean, which provides energy for the growth of waves and the development of surface currents.

*Corresponding author address: Dr. Jerome A. Smith, Marine Physical Laboratory, Scripps Institution of Oceanography, University of California at San Diego, La Jolla, CA, 92093-0213, U.S.A.

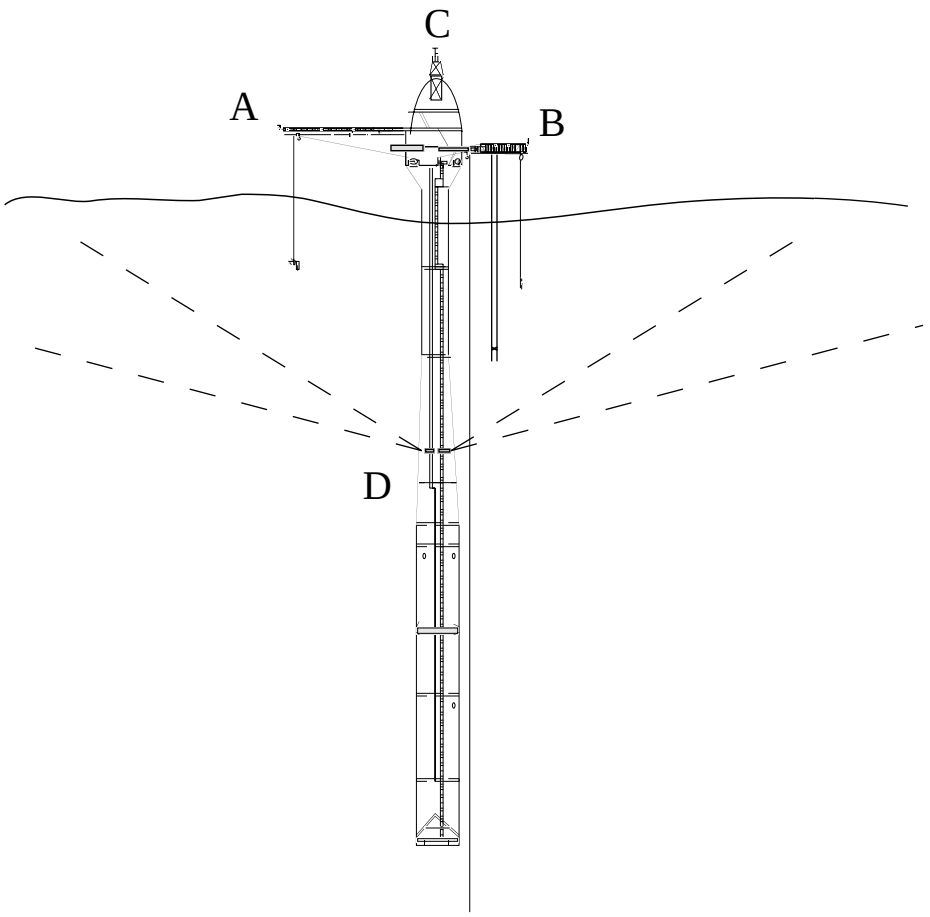

Fig. 1. Schematic view of R/P *FLIP* during SWAPP Instruments deployed included: (A,B) high frequency sonic anemometers, (C) vector-averaging wind recorder, and (D) surface scanning Doppler sonars.

The surface elevation measurements provide independent estimates of the surface waves, which are used for comparison with the sonar results. Analysis of *FLIP*'s motion itself may in theory also provide estimates of directional surface wave spectra, essentially using *FLIP* as a tilt-and-roll buoy.

A model for *FLIP*'s motion is derived by analysis of the important forces acting on the hull, and the solution of the corresponding equations for translation and rotation. With this model, a three axis accelerometer (located at 35 m depth) together with *FLIP*'s heading (measured by a gyroscope) are sufficient to estimate *FLIP*'s motion. The accelerometers measure a combination of true acceleration plus a component of gravity due to tilt. The model dynamics partition the motion between tilt and acceleration through definition of a frequency dependent center of rotation, assuming forcing by linear deep water surface gravity waves.

At times during SWAPP and previous experiments, only accelerometer and heading data are available for estimating the motion of *FLIP*. At these times, the dynamic model of *FLIP*'s motion is needed to separate the effects of tilt and acceleration. At other times, more data are available: three-axis "fluxgate" measurements (of the magnetic vector due to the earth's magnetic field), wave wire measurements (of surface elevation), and Doppler

sonar measurements of radial velocity along the surface. The additional measurements provide a basis for comparing and testing the dynamic model.

The motion of *FLIP* has been studied previously (Regier, 1975; Rudnick, 1967). However, we felt it worthwhile to re-derive the model, to provide results in forms appropriate to the available data, and also to explore the importance of some additional effects. New features of the analysis include treatment of the inertial mass of the water flowing around *FLIP* (added mass), and of skin friction effects (through a quasi-linear drag term). Inclusion of these effects may improve the performance of the model.

Several comparisons are used to test and refine the model. First, an empirical center of rotation is estimated (from a combination of accelerometer, heading, and fluxgate measurements) and is compared with the model derived center of rotation versus frequency. This comparison allows for tuning of the model. Second, the accelerometer-derived tilts of *FLIP* are compared to those calculated from fluxgate and heading data. Finally, the velocity at the sonar depth as estimated by the model is compared to the range averaged sonar velocity.

2. *FLIP* MOTION MODEL

2.1 *Formulation*

For simplicity, consider first the 2-D case, with wave forcing in just one vertical plane (x,z). Extension to the 3-D case is straightforward. We take x to be horizontal, and z vertical, increasing upwards. The horizontal motion of *FLIP* is described by the position of the center of mass, x_f, and angle of tilt from vertical, θ (assumed to be small). In general, the vertical motion of *FLIP* is less important, and is more easily estimated (e.g., by integration of the vertical component of acceleration; see appendix). The equations for translational and rotational motion are:

$$\ddot{x}_f = F/M \tag{1}$$

$$\ddot{\theta} = T/I. \tag{2}$$

Here F and T are the total force and torque on the body, respectively, and are discussed below. M and I are the total mass and the pitching moment of *FLIP*, respectively, given by:

$$M \equiv \int_{-H}^{+h} m(z)dz = \int_{-H}^{0} \rho A(z)dz \ , \tag{3}$$

$$I \equiv \int_{-H}^{h} (z - z_f)^2 m(z)dz \equiv \gamma_f^2 M, \tag{4}$$

where the depth of *FLIP*'s center of mass, z_f, is

$$z_f \equiv M^{-1} \int_{-H}^{h} z m(z)dz. \tag{5}$$

These correspond to the zeroth, second, and first moments of the vertical mass distribution of *FLIP*, respectively. In the above, H is the extent of *FLIP* in the vertical below the water line, h is the extent above water, $A(z) = \pi r^2(z)$ is the cross-sectional area of *FLIP* versus depth, $m(z)$ is the mass distribution of *FLIP* in the vertical, and γ_f is known as the radius of gyration. *FLIP*'s total mass M is equal to the displaced water mass; the radius versus depth is specified,[1] so the displacement (and hence M) is well known. However, the center of mass z_f and the radius of gyration γ_f are higher moments of the distribution of mass, $m(z)$, which are progressively more sensitive to the details of how *FLIP* is loaded. In general, these are not well known, so adjustments of z_f and γ_f are allowed, with some constraints; this is discussed below.

The forcing and motion are more easily described in the frequency domain, so Equation (1) and Equation (2) are Fourier-transformed in time. We adopt the convention of allowing only positive frequencies, so that wave direction is uniquely described by a vector wavenumber. Thus, for example, the time-series of displacement is recovered from the (hatted) frequency coefficients by

$$x_f(t) = (2/\pi)^{1/2} \int_0^\infty \hat{x}_f(\omega) e^{-i\omega t} d\omega . \tag{6}$$

We now drop the hats, and consider x_f, θ, F and T to be functions of ω.

The significant forces acting on *FLIP* include: the pressure gradient imposed by the waves; an inertial force proportional to the relative acceleration of fluid flowing around *FLIP*; a drag force acting per unit area of hull, proportional to the square of the velocity of the water relative to *FLIP*'s hull; and the vertical balance between buoyancy and weight. We neglect (for example) the wind stress acting on the portion of *FLIP* extending above water. Hence we write

$$F = F_p + \tilde{F}_i + F_d + F_b, \tag{7}$$

where the right hand terms represent forcing by the wave's pressure gradient, fluid inertia, drag, and buoyancy anomaly, respectively. The torques are separated similarly.

2.2 Wave Pressure

The pressure gradient F_p due to the waves is estimated from linear wave theory:

$$F_p(\omega) = -\rho g \eta_x \int_{-H}^{0} e^{kz} A(z) dz , \tag{8}$$

where ω is the radian frequency of the waves, $k = \omega^2/g$ is the wavenumber magnitude from linear dispersion, and $\eta_x = ik\eta$ is the (complex) surface slope at frequency ω.

[1]The radius of *FLIP* versus depth is 1.92 m from above the surface to -18.3 m depth, then increases linearly to 3.06 m at -45.7 m, and remains 3.06 m to the bottom of *FLIP* at -91.4 m.

2.3 Fluid Inertia

If *FLIP* were accelerating at exactly the same speed as the surrounding water (due to the surface wave pressure gradient), there would be no inertial effect. Only the relative acceleration of water around *FLIP*'s hull has an effect. The inertial force is often accounted for in the form of added mass, which is physically related to the volume of water distorted in flowing around the object in question. For example, with potential flow around a circular cylinder, the added mass is equal to the mass of water displaced by the cylinder (Lamb, 1932). The conceptual danger here is to neglect the fact that the water surrounding *FLIP* is already accelerating due to the exterior pressure field, and that, to some extent, *FLIP* is accelerating with it. Using linear wave theory, and neglecting the diameter of *FLIP* compared to the wavelength, the inertial force $\tilde{F}_i$ can be written in the form:

$$\tilde{F}_i(\omega) = -\rho C_i \int_{-H}^{0} \left\{ g\eta_x e^{kz} + \left(\ddot{x}_f + (z - z_f)\ddot{\theta} \right) \right\} A(z)dz \tag{9}$$

where inertial coefficient C_i is equal to the ratio of added mass to *FLIP*'s mass. Thus, for potential flow about a cylinder, C_i =1. The first term in the integrand is an additional wave force, due to the fact that the wave-induced flow must accelerate around *FLIP*. The rest is the added mass term.

It is clear from inspection of 9 that the inertial force changes the net center of mass of the system. At the net center of mass, angular acceleration should not induce translation. This occurs in 9 because the center of mass of the displaced water is at some depth z_b, rather than at the depth of *FLIP*'s center of mass, z_f. The combined mass of *FLIP* and the added mass of the water forced to flow around *FLIP* has a net center of mass at depth z_c somewhere between z_f and z_b:

$$z_c \equiv M_i^{-1} \int_{-H}^{h} z\left(m(z) + \rho C_i A(z)\right)dz = \frac{z_f + C_i z_b}{1 + C_i}, \tag{10}$$

where

$$z_b \equiv \rho M^{-1} \int_{-H}^{0} zA(z)dz \tag{11}$$

is the center of buoyancy,

$$M_i \equiv M(1 + C_i) \tag{12}$$

is the net mass including the added mass, and we make the analytic extension $A(z) \equiv 0$ from $z=0$ to $+h$, z_b. From the specified shape of *FLIP*'s hull, z_b is accurately known. At the net center of mass z_c, pure rotation and translation are uncoupled, and the net inertial force simplifies to

$$F_i(\omega) = -\rho C_i \int_{-H}^{0} \left(g\eta_x e^{kz} + \ddot{x}_c \right) A(z)dz, \tag{13}$$

where $\ddot{x}_c$ is the acceleration at z_c.

The added mass also changes the net radius of gyration. The new radius of gyration is defined by

$$\gamma_c^2 \equiv M_i^{-1} \int_{-H}^{h} (z - z_c)^2 \left(m(z) + \rho C_i A(z)\right) dz \tag{14}$$

(again, $A(z) \equiv 0$ from $z = 0$ to $+h$). This is similar in form to the Equation (4) for γ_f^2, except that the integral includes the mass distribution of the displaced water as well as that of *FLIP*, and it is referenced to z_c rather than z_f. This may be expressed in terms of z_f, z_b, γ_f^2, and the radius of gyration of the displaced water volume,

$$\gamma_b^2 \equiv \rho M^{-1} \int_{-H}^{0} (z - z_b)^2 A(z) dz. \tag{15}$$

In terms of these,

$$\begin{aligned} \gamma_c^2 &= \frac{\left(\gamma_f^2 + z_f{}^2\right) + C_i\left(\gamma_b^2 + z_b{}^2\right)}{1 + C_i} - z_c^2 \\ &= \frac{\gamma_f^2 + C_i \gamma_b^2}{1 + C_i} + \frac{C_i \left(z_b - z_f\right)^2}{\left(1 + C_i\right)^2} \end{aligned} \tag{16}$$

Since the volume distribution is known, this reduces the net sensitivity to the less well known mass distribution of *FLIP*.

The inertial force increases both the apparent mass and forcing roughly in proportion, resulting in little change in the response to waves. This accounts for the reasonable performance of models that neglected these terms. While the added mass should affect the resonant tilting period (discussed below), the error bounds on the center of mass and radius of gyration are large enough to accommodate the discrepancy.

Using the net center of mass and corresponding radius of gyration, Equation (1) and Equation (2) become

$$\ddot{x}_c = \frac{F}{M_i} \tag{17}$$

$$\ddot{\theta} = \frac{T}{M_i \gamma_c^2}. \tag{18}$$

2.4 Drag

The drag per unit area is normally assumed to have the form $-C_d |v(z)| v(z)$, where C_d is a dimensionless drag coefficient and the vector velocity v is a function of time and space. This introduces coupling between frequencies in the above equations, and makes them analytically intractable. However, a quasi-linear solution is possible, with the assumption that the coupling is weak. For small frequency bands "$d\omega$," the velocity from an individual band is always small compared to the total velocity variance. Thus, the velocity magnitude

$|v(z)|$ is roughly the total rms velocity. If there is negligible phase coupling between frequencies, then the non-linear drag force can be replaced by a quasi-linear drag, where the coefficient $V(z)$ is a function of depth and also a slow function of time:

$$D_v(z) \equiv C_d V(z). \tag{19}$$

Here C_d is the usual drag coefficient, and $V(z)$ is the root-mean-square velocity of water relative to the hull of *FLIP*. The rms velocity $V(z)$ is formed over an appropriate time interval (say, one hour). The simplest model results from setting $D_v(z)=constant$ (linear drag). This is used first to assess the qualitative effects of drag on *FLIP*'s motion. To form the depth dependent drag, we neglect the motion of *FLIP* in calculating the relative velocities, and also the details of the flow around *FLIP* (which would introduce some sensitivity to horizontal direction). $D_v(z)$ is calculated for each time period from an estimate of the 1-dimensional surface elevation frequency spectrum, using

$$V(z) \approx \sqrt{\int_0^\infty \eta(\omega)^2 \omega^2 e^{2k(\omega)z} d\omega}\,. \tag{20}$$

The exponential decay with depth makes the result insensitive to higher frequency waves. This permits the use of spectra derived from the vertical acceleration of *FLIP* (appendix). Should the drag term prove important, it might be necessary to iterate the model from Equation (20), to include the motion of *FLIP* in an improved estimate of the rms difference velocity. A mean flow can also be included in Equation (20), conceptually as a delta function at zero frequency; this could be important, since means flows over 0.2 m/s have been encountered, and the mean flow component may not decay with depth.

The area per depth increment dz is $2\pi r(z)$. Altogether, the quasi-linear drag force takes the form:

$$F_d(\omega) = 2\pi\rho \int_{-H}^{0} \left(\frac{\omega \eta_x}{ik} e^{kz} - \left(\dot{x} + (z - z_c)\dot{\theta} \right) \right) D_v(z) r(z) dz \tag{21}$$

Only the drag force is in quadrature with the surface slope η_x.

2.5 Torques

The corresponding torques are found by equations analogous to Equation (8), Equation (13), and Equation (21), but with the additional factor $(z - z_c)$ inside the depth integrals. In addition, there is a restoring force proportional to tilt, due to the fact that the center of buoyancy is above the center of mass (otherwise there would be no reason for *FLIP* to remain vertical). The torque due to the balance of buoyancy versus weight can be written

$$T_b = gM(z_b - z_f)\sin\theta \approx gM(z_b - z_f)\theta\,. \tag{22}$$

The balance between weight and buoyancy doesn't enter directly into the equations for translation at the center of mass. However, it does enter into the equation for vertical displacement (appendix A).

2.6 Solution

It is convenient to partition the forcing into a part due to the net forcing by waves, and other parts resulting from *FLIP*'s own motion. The equations for translational and rotational motion (Equation 17 and Equation 19) can be re-written in the form:

$$\ddot{x}_c = \eta_x F_w - d_{xx}\dot{x}_c - d_{x\theta}\dot{\theta} \ , \tag{23}$$

$$\ddot{\theta} = \eta_x T_w - d_{\theta x}\dot{x}_c - d_{\theta\theta}\dot{\theta} - b_\theta \theta, \tag{24}$$

where $\eta_X(w)$ is the (complex) wave slope amplitude; F_w and T_w are defined as the net forcing and torque (respectively) applied per unit wave slope, normalized by the corresponding inertial moments (including the added mass); the d_{nm} are various quasi-linear drag components; and b_θ is the buoyant restoring force working against tilting of *FLIP*. From Equation (8), Equation (13), and Equation (21) and the torque analogs:

$$F_w = \frac{-\rho g}{M_i}\int_{-H}^{0}\left\{A(z)\left(1+C_i\right)+i\frac{2\pi r(z)D_v(z)}{\omega}\right\}e^{kz}dz \tag{25}$$

$$T_w = \frac{-\rho g}{M_i\gamma_c^2}\int_{-H}^{0}\left\{A(z)\left(1+C_i\right)+i\frac{2\pi r(z)D_v(z)}{\omega}\right\}(z-z_c)e^{kz}dz \tag{26}$$

$$d_{xx} = \frac{2\pi\rho}{M_i}\int_{-H}^{0} D_v(z)r(z)dz \tag{27}$$

$$d_{x\theta} = \frac{2\pi\rho}{M_i}\int_{-H}^{0}(z-z_c)D_v(z)r(z)dz \tag{28}$$

$$d_{\theta x} = \frac{2\pi\rho}{M_i\gamma_c^2}\int_{-H}^{0}(z-z_c)D_v(z)r(z)dz = \gamma_c^{-2}d_{x\theta} \tag{29}$$

$$d_{\theta\theta} = \frac{2\pi\rho}{M_i\gamma_c^2}\int_{-H}^{0}(z-z_c)^2 D_v(z)r(z)dz \tag{30}$$

$$b_\theta = \frac{g(z_b - z_f)}{(1+C_i)\gamma_c^2}. \tag{31}$$

Solutions to these equations of motion are sought for x_c and θ as functions of frequency (i.e., looking for solutions proportional to $e^{-i\omega t}$), with the result:

$$x_c = \eta_x\left(\frac{d_{x\theta}T_w + i\omega^{-1}(\omega^2 + i\omega d_{\theta\theta} - b_\theta)F_w}{(d_{xx}-i\omega)(\omega^2 + i\omega d_{\theta\theta} - b_\theta) - i\omega d_{\theta x}d_{x\theta}}\right) \equiv \eta_x X \tag{32}$$

$$\theta = \eta_x \left(\frac{d_{\theta x} F_w - (d_{xx} - i\omega) T_w}{(d_{xx} - i\omega)(\omega^2 + i\omega d_{\theta\theta} - b_\theta) - i\omega d_{\theta x} d_{x\theta}} \right) \equiv \eta_x \Theta . \tag{33}$$

Within the approximations used, the same formulation applies to the *y*-component: the response *Y* to a unit amplitude wave traveling in the *y* direction is equal to the response *X* to another unit amplitude wave traveling in the *x* direction. For small tilts, the tilt θ in the *x*-*z* plane and ϕ in the *y*-*z* plane (say) may be treated as independent (approximately Cartesian); in this case, the formal equivalence applies between Θ and Φ as well. In general, the tilts of *FLIP* are small enough that this is a good approximation. The equivalence of *x* and *y* responses also depends on the assumption that the quasi-linear drag is horizontally isotropic.

For real ω and no forcing, the solution goes to zero. Physically, damping (the d_{nm} terms) excludes the possibility of unforced motions having the assumed time-dependence (steady oscillations). Solutions of the unforced (homogeneous but coupled) equations can be found as the zeros of the denominator common to Equation (32) and Equation (33), allowing the frequency ω to be complex. This leads to solutions in the form of damped oscillations. For the present purposes, such homogeneous solutions are assumed to have decayed to nothing. There remain near-resonances, yielding large amplitude responses to forcing at (real) frequencies near these (complex) values. This fact is used later to help refine the ill-known parameters z_f and γ_f.

When damping is negligible, the solution simplifies considerably. in this case, Equation (32) and Equation (33) simplify to

$$x = -\eta_x \omega^{-2} F_w \tag{34}$$

$$\theta = \frac{-\eta_x T_w}{(\omega^2 - b_\theta)} . \tag{35}$$

The homogeneous solution for θ is simple harmonic motion with frequency $\omega_R \approx \sqrt{b_\theta}$.

2.7 Implementation

We now turn to constraints on *FLIP*'s center of mass z_f and the radius of gyration γ_f. Both depend on the loading of *FLIP*. As a starting point, Regier (1975) quoted values of z_f=56 m and γ_f=25.6 m. Since 1975, *FLIP* has undergone some reconstruction, which could change the estimates of z_f and γ_f. For example, while Regier reported a resonant tilting period of 47 seconds in 1975, the data from SWAPP indicates a resonant period of 58 seconds. As noted above, the resonance can be found from the zeros of the denominator common to both Equation (32) and Equation (33), leading to a cubic equation in ω. However, for the present purpose, the resonant tilting period is specified much more easily from the undamped solution:

$$T_{res} \equiv \frac{2\pi}{\omega_R} \approx \frac{2\pi}{\sqrt{b_\theta}} \approx 2\pi\gamma_c \sqrt{\frac{(1+C_i)}{g(z_b - z_f)}} . \tag{36}$$

Since the volume moments z_b and γ_b are known, and T_{res} can be specified from the data, the result is a constraint on the joint variations of z_f and γ_f: these must vary together

so as to reproduce the observed resonant period. (Another constraint, that $z_b > z_f$, is also enforced by this equation.)

We choose to specify γ_f, and find z_f from the solution of the quadratic equation resulting from Equation (36) and Equation (16)

$$z_f = z_b - \frac{\left(g\omega_R^{-2}\right) - \sqrt{\left(g\omega_R^{-2}\right)^2 - 4\left(\frac{C_i}{1+C_i}\right)\left(\gamma_f^2 + C_i\gamma_b^2\right)}}{2\left(\frac{C_i}{1+C_i}\right)}. \tag{37}$$

(We take the smaller solution. The other solution corresponds to the unphysical case of z_f and z_b so far apart that the increase in γ_c overwhelms the increase in restoring force. Note that $g\omega_R^{-2}$ is of order 1 km, while γ_f and γ_b are 20 to 30 m.)

There are three adjustable parameters: the inertial mass ratio C_i (which we shall take to be 1.0), the drag coefficient C_d, and the combination of γ_f and z_f which does not change the resonant period. In fact, fixing the inertial mass ratio to 1.0 is acceptable since, by inspection of the forcing equations, a change in C_i has an effect equivalent to changes in C_d and γ_f; thus, it does not introduce any new degrees of freedom. The remaining two parameters can be adjusted (within reasonable bounds) to find values providing the best fit between the various kinds of data, over a variety of environmental conditions.

The purpose of this model is to permit estimation of *FLIP*'s motion from a reduced set of measurements; e.g., from just accelerometer measurements at 35m depth and heading. The model partitions the motion of *FLIP* between tilt and the acceleration measured at any specified depth. A simple way to visualize this partitioning is that the model specifies a center of rotation at each frequency in response to the forcing by a free gravity wave. Thus, at a given depth, the ratio between horizontal displacement and tilt is set, for each frequency, by the distance from the center of rotation.

Conceptually, the center of rotation is the depth at which the centerline of *FLIP* remains fixed horizontally. In practice, the presence of the drag force makes this complex; however, the concept remains useful, especially since the drag is small. For small tilts, the center of rotation is approximately

$$z_r(\omega) = z_c - X(\omega)/\Theta(\omega). \tag{38}$$

3. COMPARISONS

3.1 Data and Calibrations

The fluxgate measures the 3 component magnetic flux vector of the earth's magnetic field. Unfortunately, the vertical fluxgate channel was faulty. Fortunately, at 35°N the magnetic flux lines are quite steep (~60° from horizontal), so the tilt in the horizontal plane can still be resolved, given an independent measurement of heading (such as that provided by the gyrocompass). However, the calibration of the flux measurements are in doubt. At low frequencies, the accelerometer readings are dominated by gravity times tilt, so we use the low-frequency accelerometer data to calibrate the fluxgates.

The accelerometer data was checked first for self-consistency. Two minute averages were formed, and the magnitudes were checked against the known value of gravity. Next, tilts calculated from the accelerometers were compared with tilts estimated from the wave

wires, first using the measured distances of each wire from the axis of *FLIP*, and then using the low-frequency mean (two-minute) tilts over the three wire array, which forms a triangle 1 meter on a side. The latter estimate of tilt has less resolution than the first, but provides a check on the component of tilt perpendicular to the orientation of the boom.

Having confirmed the accelerometer calibrations in some detail, the fluxgate data was then post-calibrated via two models, incorporating both heading and accelerometer-derived tilts: (1) a direct least-squares-fit linear model from the raw fluxgate readings to heading and tilt, and (2) a geometric model, which included the measured geometry of the experimental setup, including boom tilt, orientation, and twist. In the magnetic North-South direction, the resulting data agree well via either model, but in the East-West direction, the geometric model fares somewhat worse than the direct linear fit. This indicates that some unknown effect may be degrading the E-W result. For this reason, only N-S components of the data are used in the comparison with the *FLIP* motion model.

Sample N-S and E-W accelerometer and fluxgate equivalent spectra are shown in Figure 2, extending up through the wave frequencies. As enforced by calibration, the accelerometer and fluxgate spectra are nearly identical at low frequencies (particularly at the tilt resonant frequency of .017, corresponding to a period of 58 seconds). However, at high frequencies the effect of waves accelerating *FLIP* can be seen clearly: at the peak wave frequencies, power in the accelerometer measurements is close to an order of magnitude greater than that of the fluxgate. As well, the noisy nature of the fluxgate data is shown by the noise floor extending above 0.2 Hz.

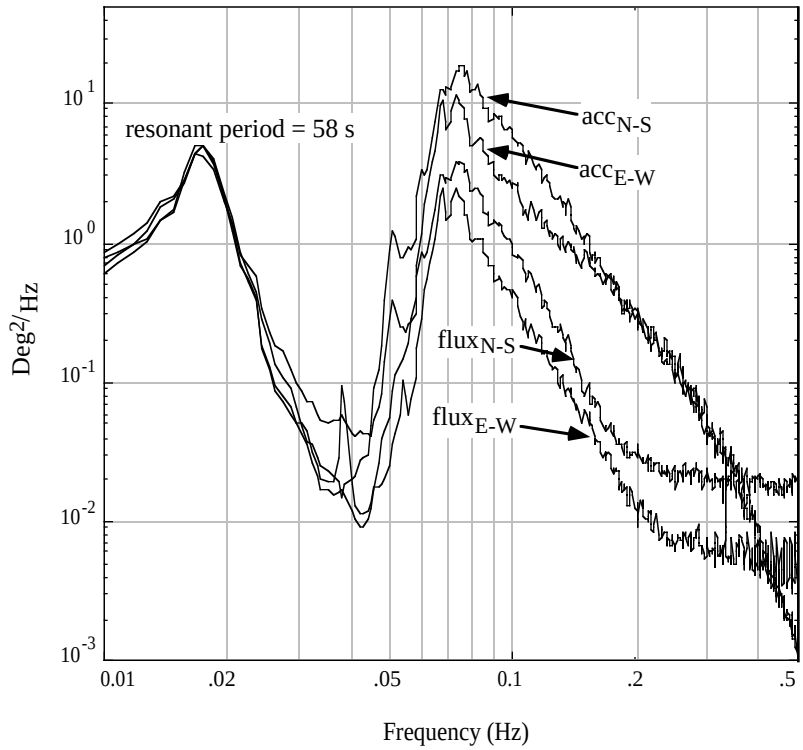

Fig. 2. North-South and East-West (acc) accelerometer and (flux) fluxgate equivalent spectra As enforced by calibration, the spectra match at the tilt resonant period of 58 seconds, but at higher frequencies, the effect of waves, which accelerate *FLIP*, can clearly be seen.

3.2 Empirical Motion and Model Tuning

With accelerometer, fluxgate, and gyroscope measurements, an empirical center of rotation can be calculated. The accelerometer measurements combine true acceleration at a known depth (z_a=35 m) and a component of gravity due to tilt. For example, the x-component of the accelerometer measurement is

$$a_x \approx \ddot{x}_a - g\sin\theta = \ddot{\theta}(z_r - z_a) - g\sin\theta \tag{39}$$

where x_a is the horizontal displacement at the depth of the accelerometer, z_a, and z_r is (again) the center of rotation. For small tilts, $sin\theta \approx \theta$, the displacement and tilt can be combined in a manner analogous to 38 to obtain an empirical center of rotation from a combination of accelerometer (a) and fluxgate (θ) measurements:

$$z_r = z_a + \omega^{-2}\left(g + a/\theta\right). \tag{40}$$

The comparison between empirical and modeled center of rotation (as functions of ω) allows a method by which to evaluate the model and set the free parameters.

Within the region of high surface wave energy (above .05 Hz) the effect of drag is minimal. At lower frequencies, increasing the drag (C_d = 0.0 to 0.5) deepens the center of rotation, such that motion of *FLIP* is more translational than rotational. Also, increasing the drag from zero quickly suppresses the tilt resonance. We deduce from Figure 2 that the system has little drag. Within the wave band, drag can be ignored.

Variation of the radius of gyration alters the shape and position of the center of rotation curve across a wide range of frequencies. This is seen in Figure 3, where the empirical and modeled center of rotation (for values of γ_f = 17, 19, and 21 and zero drag) have been plotted. Increasing γ_f moves the center of rotation away from the center of mass, while decreasing it moves the center of rotation asymptotically closer to the net center of mass, z_c. Also, as the surface wave frequency increases, the forcing becomes localized at the surface, and the center of rotation approaches a fixed level. Within the constraints of the physics included in the model (e.g., a rigid hull forced by surface waves), the center of rotation is always shallower than the net center of mass.

The modeled center of rotation for γ_f=19 fits the empirical curve best in the range of the most energetic waves (frequencies between .08 and .10 Hz). This value is lower than that suggested by Regier (1975), 25.6 m, but is within reason, especially considering modifications made to *FLIP* since then.

3.3 Tilt Comparison

Tilt can be obtained from accelerometer data, using the model center of rotation from above:

$$\theta = \frac{x_a}{(z_a - z_r)} = \frac{-a_x}{\omega^2(z_a - z_r) + g} \tag{41}$$

(the same formulation applies to the x and y-components). To compare with measured tilt, two time segments are chosen. At these two times (March 11, 1990 to March 13, 1990), all the relevant data are available, and two different conditions are represented. The modeled tilt in the N-S plane (Figure 4) show good agreement with the magnetic flux tilt measurement in phase, and compare favorably in amplitude as well, with errors of

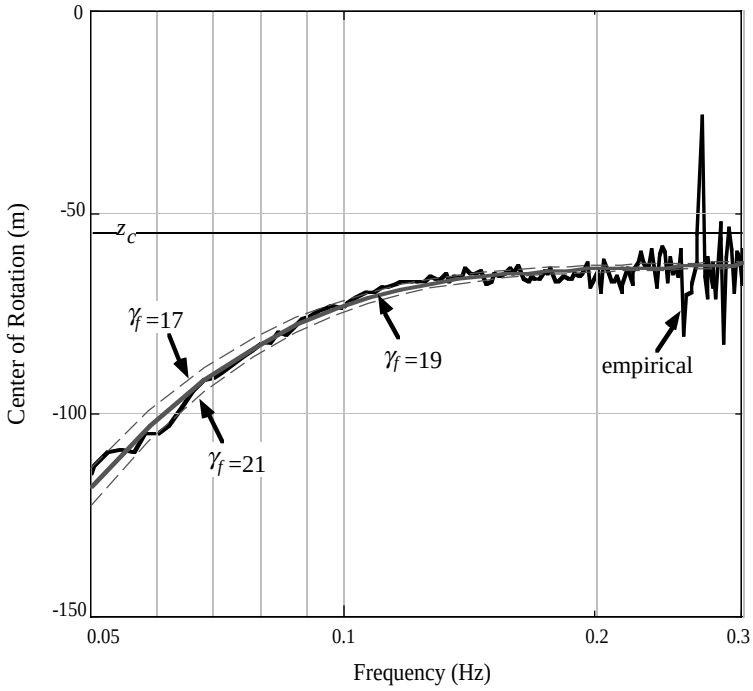

Fig. 3. (Grey) model and (black) empirical center of rotations vs. frequency. The model derived center of rotation was calculated for various radii of gyration (γ_f = 17, 19, and 21 m). The model with radius of gyration = 19 m (solid) is seen to fit the empirical data best in the range of the most energetic waves. Larger radii move the center of rotation away from the center of mass. For low frequency waves, whose effective forcing occurs further below the sea surface, the center of rotation is deeper. In contrast, for high frequency waves, whose effective forcing approaches the sea surface, the center of rotation assymptotically approaches some depth below the center of mass.

17.6% and 24.6% of the total variance respectively. The noise in the fluxgate signal is partially responsible for the calculated error.

3.4 Velocity Comparison

Our intended use of the motion model is to correct velocity estimates from a Doppler sonar system mounted at 35 m depth on *FLIP's* hull. For comparison, the mean velocity over a suitable range away from *FLIP* (80 to 300 m) is used to indicate the motion of the sonar (and hence of *FLIP* at that depth) relative to the water. In SWAPP this velocity is available every 1.5 seconds.

As noted above, the accelerometer measurements correspond to a combination of true acceleration and a component of gravity due to tilt. Making the small angle approximation, and using the center of rotation (38) to convert angle to displacement, the displacement of *FLIP*'s hull at the depth of the accelerometers can be written

$$x_a = \frac{-a_x}{\omega^2 + g/(z_a - z_r)}. \tag{42}$$

This is most easily done in the frequency domain, since z_r is a function of frequency. Horizontal displacement can be computed anywhere along *FLIP*'s hull, using the center of rotation as in Equation (42). Displacements can be converted to velocity, via multiplication by $-i\omega$.

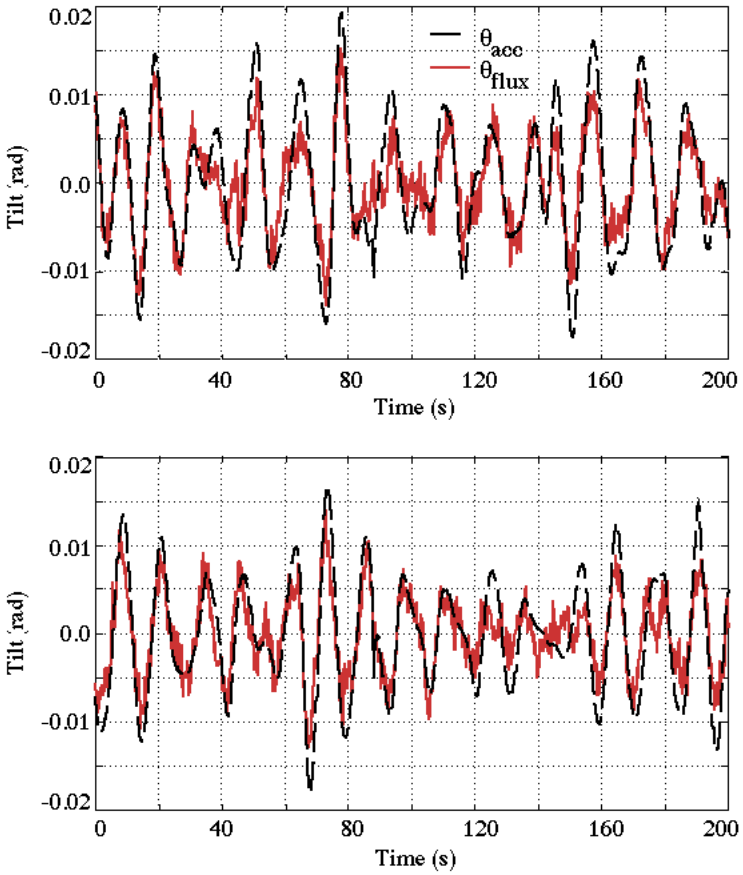

Fig. 4. Time-series of (grey) accelerometer-derived tilt, via *FLIP* motion model, and (black) fluxgate measured tilt, for two time periods: (top) March 11, 1990, 20:29, and (bottom) March 13, 1990, 1:47.

The model and sonar velocities have been filtered by a fourth order Butterworth high pass filter to frequencies above .05 Hz. The resulting time-series (Figure 5) show good agreement, with errors of 15.7% and 15.0% of the total variance, respectively.

4. Conclusions

The most fundamental aspects of *FLIP* motion are well described by this linear model. By the calculation of a frequency dependent center of rotation, the model allows the accelerometer measurements to be partitioned between tilt and acceleration, thus allowing the estimation of motion at any point on the *FLIP* superstructure. Comparisons with independent data have shown that the modeled response of *FLIP* matches the actual response to within the accuracy necessary for the purposes here. Sonar and model derived estimates of velocities at the sonar depth show good agreement both in magnitude and phase. The tilting of *FLIP* is also modeled well, as indicated by the comparison with data from a geomagnetic vector pointer.

The estimates of acceleration and tilt may now be used to determine the effects of *FLIP* motion on the various measurements taken from the superstructure. One important example is the measurement of the wind stress. For a sample period (March 11, 20:29) the vertical and horizontal root mean square velocities of the sonic anemometer due to *FLIP* motion

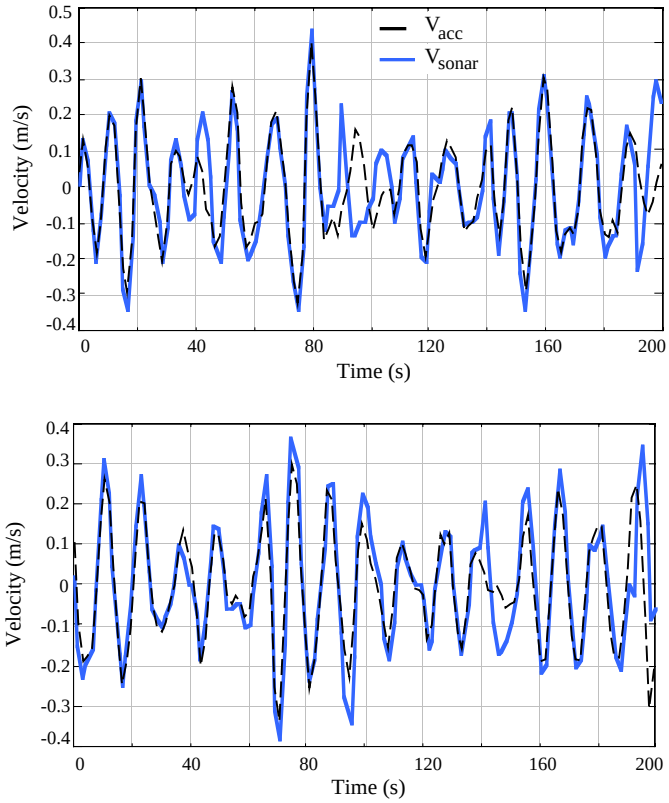

Fig. 5. Time-series of (grey) accelerometer-derived velocity at the sonar depth, via *FLIP* motion model, and (black) the sonar range-mean velocity for two time periods: (top) March 11, 1990, 20:29, and (bottom) March 13, 1990, 1:47.

are estimated at .03 and .15 m/s respectively. However, since the tilt and rotation resonances are quite different, the induced vertical and horizontal velocities are poorly correlated (correlation coefficient of r^2=.03). The resultant wind stress contribution is estimated to be 8.8×10^{-4} N/m^2, more than two orders of magnitude smaller than the measured wind stresses. Indeed, *FLIP* **is** a stable platform.

Acknowledgments: We would like to thank E. Slater, L. Regier, and R. Pinkel for useful discussions about FLIP's motion and ballasting. Thanks to Lloyd Green, Mike Goldin, and Chris Neely for help with the instrumentation and calibration. Also, thanks to E. DeWitt and the crew of FLIP for their help during the deployment. This research was supported by the Office of Naval Research and the Mineral Management Service, under contracts N00014-90-J-1285, N00014-93-1-0359, and N00014-93-1-1157.

REFERENCES

Lamb, H., *Hydrodynamics* (6th edition), Reprinted with permission in 1945 by Dover publications, New York, NY, 1932.

Regier, L., Observations of the Power and Directional Spectrum of Oceanic Surface Waves, PhD. Thesis, Scripps Institution of OceanographyUniversity of California, San Diego, 1975.

Rudnick, P., Motion of a Large Spar Buoy in Sea Waves, *J. Ship. Res.*, *11*, 257-267, 1967.

Smith, J. A., Observed Growth of Langmuir Circulation, *J. Geophys. Res.*, *97*, 5651-5664, 1992.

Smith, J. A., and G. T. Bullard, Directional Surface Wave Estimates from Doppler Sonar Data, *J. Atmos. Oceanic Technol.*, *12*, 617-632, 1995.

Weller, R. A., M. A. Donelan, M. G. Briscoe, and N. E. Huang, Riding the Crest: A Tale of Two Wave Experiments, *Bull. Amer. Meteor. Soc.*, *72*, 163-183, 1991.

APPENDIX

One significant force acting to move *FLIP* vertically is pressure, in response to the fluctuating sea surface height:

$$F_z \approx \rho g k \eta \int_{-H}^{0} e^{kz} A(z) dz \,. \tag{43}$$

For flow parallel to a cylinder, the inertial force is negligible. The drag force has the same form as in the horizontal case, but the coefficient is not necessarily the same. We shall neglect it here. The other important forces are the restoring force brought about by buoyancy, balanced against the weight of *FLIP*:

$$F_b \approx \rho g \int_{-H+z}^{0} A(z'-z) dz' - M = -z(\rho g A_0) \tag{44}$$

where A_0 is the cross-sectional area of *FLIP* at the mean waterline (*FLIP* is uniform in cross-section over several meters on either side of the mean waterline).

An estimate of the vertical motion of *FLIP* is given by the solution of the equation

$$M\ddot{z} = F_z + F_b = \rho g k \eta \int_{-H}^{0} e^{kz} A(z) dz - \rho g z A_0 \tag{45}$$

or

$$a_z \equiv \ddot{z} = \eta \frac{\rho g k \int_{-H}^{0} e^{kz} A(z) dz}{\left(M - \rho g \omega^{-2} A_0\right)}, \tag{46}$$

where a_z is the vertical component of acceleration measured along *FLIP*'s centerline. Thus, a wave spectrum estimate is given by

$$S(f) \equiv |\eta|^2 = \frac{|a_z|^2}{\omega^4} \left(\frac{M - \rho g \omega^{-2} A_0}{\rho \int_{-H}^{0} e^{kz} A(z) dz} \right)^2 . \tag{47}$$

The solution 46 has a resonance at $\omega^2 = \rho g A_0 / M$. For *FLIP*, this resonance occurs at a period of about 26 seconds.